Title

Flow-mediated modulation of the endothelial cell lipidome

Authors

Hong, Soon-Gook
Kennelly, John P
Williams, Kevin J
et al.

Publication Date

2024

DOI

10.3389/fphys.2024.1431847

Peer reviewed

frontiers | Frontiers in Physiology

TYPE Original Research
PUBLISHED 24 July 2024
DOI 10.3389/fphys.2024.1431847

OPEN ACCESS

EDITED BY
Markus Hecker,
Heidelberg University, Germany

REVIEWED BY
Thomas Korff,
Heidelberg University, Germany
Andreas H. Wagner,
Heidelberg University, Germany

*CORRESPONDENCE
Julia J. Mack,
jmack@mednet.ucla.edu

RECEIVED 13 May 2024
ACCEPTED 01 July 2024
PUBLISHED 24 July 2024

CITATION
Hong S-G, Kennelly JP, Williams KJ, Bensinger SJ and Mack JJ (2024), Flow-mediated modulation of the endothelial cell lipidome.
Front. Physiol. 15:1431847.
doi: 10.3389/fphys.2024.1431847

Flow-mediated modulation of the endothelial cell lipidome

Soon-Gook Hong[1,2], John P. Kennelly[2,3], Kevin J. Williams[4,5], Steven J. Bensinger[5,6] and Julia J. Mack[1,2]*

[1]Department of Medicine, Division of Cardiology, University of California, Los Angeles, Los Angeles, CA, United States, [2]Molecular Biology Institute, University of California, Los Angeles, Los Angeles, CA, United States, [3]Department of Pathology and Laboratory Medicine, University of California, Los Angeles, Los Angeles, CA, United States, [4]Department of Biological Chemistry, University of California, Los Angeles, Los Angeles, CA, United States, [5]UCLA Lipidomics Lab, University of California, Los Angeles, Los Angeles, CA, United States, [6]Department of Microbiology, Immunology and Molecular Genetics, University of California, Los Angeles, Los Angeles, CA, United States

The luminal surface of the endothelium is exposed to dynamic blood flow patterns that are known to affect endothelial cell phenotype. While many studies have documented the phenotypic changes by gene or protein expression, less is known about the role of blood flow pattern on the endothelial cell (EC) lipidome. In this study, shotgun lipidomics was conducted on human aortic ECs (HAECs) exposed to unidirectional laminar flow (UF), disturbed flow (DF), or static conditions for 48 h. A total of 520 individual lipid species from 17 lipid subclasses were detected. Total lipid abundance was significantly increased for HAECs exposed to DF compared to UF conditions. Despite the increase in the total lipid abundance, HAECs maintained equivalent composition of each lipid subclass (% of total lipid) under DF and UF. However, by lipid composition (% of total subclass), 28 lipid species were significantly altered between DF and UF. Complimentary RNA sequencing of HAECs exposed to UF or DF revealed changes in transcripts involved in lipid metabolism. Shotgun lipidomics was also performed on HAECs exposed to pro-inflammatory agonists lipopolysaccharide (LPS) or Pam3CSK4 (Pam3) for 48 h. Exposure to LPS or Pam3 reshaped the EC lipidome in both unique and overlapping ways. In conclusion, exposure to flow alters the EC lipidome and ECs undergo stimulus-specific lipid reprogramming in response to pro-inflammatory agonist exposure. Ultimately, this work provides a resource to profile the transcriptional and lipidomic changes that occur in response to applied flow that can be accessed by the vascular biology community to further dissect and extend our understanding of endothelial lipid biology.

KEYWORDS

shear stress, flow pattern, endothelial cell, lipid profile, inflammation

1 Introduction

Endothelial cells (ECs) line the luminal surface of the vasculature and are constantly exposed to mechanical forces generated by blood flow (Galley and Webster, 2004). Due to variations in vessel geometry and curvature, the arterial endothelium experiences different blood flow patterns, including unidirectional laminar flow (UF) generated in linear regions of the vasculature and oscillatory disturbed flow (DF) in regions of the vasculature that are highly curved or bifurcated (Malek et al., 1999). Different levels of hemodynamic shear stress (the frictional force acting on ECs) are present and range from high arterial shear stress

(>15 dyne/cm^2) induced by UF to low time-averaged shear stress (4 dyne/cm^2) and oscillating flow direction induced by DF.

These distinct blood flow patterns are known to induce different EC phenotypes. While UF promotes a state of endothelial quiescence and an anti-inflammatory phenotype, a pro-inflammatory phenotype is associated with ECs exposed to DF (Chiu and Chien, 2011). Therefore, exposure to DF presents as a local risk factor for vascular inflammation and disease progression (Davis et al., 2001; Yurdagul et al., 2016). Furthermore, the endothelium exposed to DF is more susceptible to the development of chronic inflammatory diseases such as atherosclerosis (Malek et al., 1999; Yurdagul et al., 2016).

Lipids are a major class of biological molecules that are essential for cellular function. Lipids are involved in many bioenergetic, biochemical, and biophysical processes (Muro et al., 2014) and so maintaining lipid homeostasis is critical to cellular health. All cellular membranes are composed of lipids, predominantly phospholipids including glycerophospholipids and sphingolipids (Mutlu et al., 2021; Sakuragi and Nagata, 2023). Neutral lipids, including triglycerides (TG) and cholesteryl esters, are also stored in cytosolic lipid droplets surrounded by a monolayer of phospholipids (Goodman, 2008). In ECs, it has been demonstrated previously that mechanical forces due to applied flow affect the membrane lipid order and fluidity (Yamamoto and Ando, 2013) and alter membrane cholesterol levels (Yamamoto et al., 2020). However, a comprehensive assessment of the changes that occur to the EC lipidome in response to mechanical stress is lacking. In the last decades, many studies have set out to understand the mechanisms of EC inflammatory activation and to identify molecular pathways and potential therapeutic targets to alleviate vascular inflammation (Immanuel and Yun, 2023). However, the role of membrane lipids in the context of EC signaling and vascular inflammation has been less studied.

Here, we conducted complementary studies to characterize the transcriptional and lipidomic profiles of human aortic ECs (HAECs) exposed to the physiological flow conditions of UF and DF. We further compared these datasets to the lipidomic signatures of HAECs exposed to pro-inflammatory agonists. Our results provide a resource to examine how blood flow pattern affects the EC lipid profile and enable the identification of lipid species involved in endothelial inflammation and vascular disease.

2 Methods

2.1 Cell culture and flow application

Primary HAECs (Cell Applications #S304-05a, Lot#1487(s); healthy normal human aorta from 21-year-old Caucasian male) were used from P4 to P12. For cell culture experiments, MCDB-131 complete media (VEC Technologies #MCDB-131 Complete) was supplemented with 10% FBS (Omega USDA certified FBS #FB-11). For plating cells on cell culture dishes, 0.1% gelatin (Stemcell #07903) coating was first applied. Cells were cultured in a 37 °C incubator with 5% CO_2. For application of shear stress, HAECs were seeded in ibidi μ-Slide 0.2 (ibidi #80166) or 0.6 (ibidi #80186) Luer ibiTreat. Unidirectional laminar flow (20 dyn/cm^2) or disturbed flow (±4 dyn/cm^2, 2 Hz) was applied to confluent monolayers using the ibidi pump system (ibidi #10902).

2.2 RNA sequencing analysis

HAECs were seeded on ibidi μ-Slides and subjected to unidirectional laminar flow (20 dyn/cm^2) or disturbed flow (±4 dyn/cm^2, 2 Hz) using the ibidi pump system for 48 h in a 37°C incubator with 5% CO_2. After 48 h, cells were washed with 1X PBS (Gibco #14190-144) and then lysed using RLT lysis buffer (QIAGEN #79216) plus 1% 2-Mercaptoethanol (Sigma Aldrich #M6250). For each condition, four μ-Slides were combined as one flow-exposed sample for a total of 12 slides for n = 3 samples. RNA extraction, library construction, and sequencing were conducted by the UCLA Technology Center for Genomics & Bioinformatics (TCGB) core facility.

Briefly, libraries for RNA sequencing were prepared with KAPA Stranded mRNA-Seq Kit (KAPA Biosystems #KK8421). Briefly, the workflow consisted of mRNA enrichment and fragmentation, first strand cDNA synthesis using random priming followed by second strand synthesis converting cDNA:RNA hybrid to double-stranded cDNA (ds-cDNA), and incorporation of dUTP into the second cDNA strand. cDNA generation was followed by end repair to generate blunt ends, A-tailing, adaptor ligation and PCR amplification. Different adaptors were used for multiplexing samples in one lane. Sequencing was performed on Illumina HiSeq 3,000 for SE 1 × 65bp run. Data quality check was done on Illumina SAV. Demultiplexing was performed with Illumina Bcl2fastq v2.19.1.403 software. The alignment was performed with Spliced Transcripts Alignment to a Reference (STAR) (Dobin et al., 2013) using the human reference genome assembly GRCh38. The Ensembl Transcripts release GRCh38.107 GTF was used for gene feature annotation. For normalization of transcript counts, normalized counts were generated by counts per million (CPM) normalization.

For graphical display of differential expression, Heatmapper (Babicki et al., 2016) was used to create a heatmap of gene expression. Average linkage was used as Clustering Method, and Kendall's Tau was used as Distance Measurement Method. VolcaNoseR was used to generate the Volcano plot of gene expression. Log_2 (fold change; FC) as X-variables and −log10 (p-value) as Y-variables were used. ShinyGO 0.77 (Ge et al., 2020) was used for gene enrichment analysis with false discovery rate (FDR) of 0.05 as cut-off. The Database for Annotation, Visualization and Integrated Discovery (DAVID, NIH) was used to identify the biological pathways enriched under DF *versus* UF. Principal component analysis (PCA) was conducted using ClustVis (Metsalu and Vilo, 2015).

Gene Set Enrichment Analysis (GSEA) 4.3.2 software was used to identify biological pathways enriched in response to DF. Genes used for GSEA were those that were differentially expressed in HAECs under DF *versus* UF. The Hallmarks gene set database was used with the following analysis parameters: Number of permutations: 1,000; Collapse/Remap to Gene Symbols: No Collapse; Permutation type: Gene Set; Chip Platform: Human Gene Symbol with Remapping MSigDB.v2023.1. Hs.chip; Enrichment Statistic: Weighted; Metric for Ranking Genes: Signal2Noise; Gene List Sorting Mode: Real; Gene List Ordering Mode: Descending; Max Size: Exclude Larger Sets: 500; Min Size: Exclude Smaller Sets: 15.

From the Gene Ontology (GO) database, lists of genes involved in lipid catabolic process (GO:0016042), neutral lipid catabolic process (GO:004646), and fatty acid catabolic process (GO:

0009062) were identified, and gene expression levels analyzed, from the RNAseq dataset.

2.3 Lipidomics analysis

For flow experiments, HAECs were seeded on ibidi μ-Slides and subjected to unidirectional laminar flow (20 dyn/cm^2) or disturbed flow (±4 dyn/cm^2, 2 Hz) using the ibidi pump system for 48 h in a 37°C incubator with 5% CO_2. After 48 h, cells were washed with ice-cold 1X PBS and subjected to trypsinization for cell detachment from the slide. For each flow condition, 3 μ-Slides were combined as one sample for a total of 9 slides for n = 3 samples. For inflammatory agonist treatments, HAECs were seeded to confluence on 6-well plates (Corning #353046) and treated with either LPS (50 ng/mL; Invivogen, #tlrl-smlps), Pam3 (200 ng/mL; Invivogen #tlrl-pms), or vehicle control for 48 h. Cells were collected and resuspended after centrifugation at 900 rpm for 5 min at 4°C. Cell number was assessed by hemocytometer. Lipid extraction and analysis were conducted by the UCLA Lipidomics Lab.

Cells were transferred to extraction tubes with 1X PBS. A modified Bligh and Dyer extraction (Hsieh et al., 2021) was carried out on samples. Prior to biphasic extraction, a standard mixture of 75 lipid standards (Avanti #330820, 861809, 330729, 330727, 791642) was added to each sample. Following two successive extractions, pooled organic layers were dried down in a Thermo SpeedVac SPD300DDA using ramp setting 4 at 35°C for 45 min with a total run time of 90 min. Lipid samples were resuspended in 1:1 methanol/dichloromethane with 10 mM ammonium acetate and transferred to robovials (Thermo #10800107) for analysis.

Samples were analyzed by direct infusion on a Sciex 5,500 with Differential Mobility Device (DMS) —comparable to the Sciex Lipidyzer platform—with a targeted acquisition list consisting of 1,450 lipid species across 17 subclasses. The DMS was tuned with EquiSPLASH LIPIDOMIX (Avanti #330731). Data analysis was performed with in-house data analysis workflow. All instrument settings, MRM lists, and analysis methods are available (Su et al., 2021). Quantitative values were normalized to cell counts.

Heatmaps were generated using Heatmapper (Babicki et al., 2016) and ClustVis (Metsalu and Vilo, 2015). Principal component analysis (PCA) was conducted using ClustVis. *X* and *Y*-axis show principal component 1 (PC1) and principal component 2 (PC2), respectively. PCA loadings were extracted from the ClustVis, and the top 20 loadings for PC1 were identified. Cross analysis of the datasets was conducted using InteractiVenn (Heberle et al., 2015) to identify lipid species that were changed under DF and pro-inflammatory agonist exposure.

2.4 Gene expression analysis

For gene expression analysis using qPCR, total RNA was extracted from HAECs using RNeasy Mini kit (QIAGEN #74104). RNA was converted to cDNA by reverse transcription, and cDNA was quantified using a Nano-Drop 8,000 (Thermo Fisher). Target genes were quantified using iTaq universal SYBR Green Supermix (BioRad #1725125) and the appropriate primer pairs. Samples were run on a QuantStudio 6 Flex 384-well qPCR apparatus (Applied Biosystems). Each target gene was normalized to HPRT. Primer sequences (5′– 3′) are listed below.

KLF2 CATCTGAAGGCGCATCTG CGTGTGCTTTCGGTAGTGG.
KLF4 AGAGTTCCCATCTCAAGGCA GTCAGTTCATCTGAGCGGG.
HPRT GCCCTGGCGTCGTGATTAGT AGCAAGACGTTCAGTCCTGTC.
NOS3 GGATGTGGCTGTCTGCATGGAC TGGTCCACGATGGTGACTTTGG.

2.5 Immunostaining and confocal imaging

For immunostaining, HAECs were fixed with 4% PFA for 5 min followed by multiple washes with 1X PBS. Samples were then blocked for 1 h with 5% Normal donkey serum (Jackson Immuno Research Laboratories #017-000-121) in 1X PBS. Then, samples were permeabilized with 0.1% Triton X-100 (Fisher Scientific #A16046-0F) for 5 min followed by blocking with 5% Normal donkey serum for 1 h. Primary antibodies were incubated overnight at 4 °C in blocking buffer and secondary antibodies applied for 1 h at room temperature. Primary antibodies used: NOS3 (Santa Cruz #sc-376751), ICAM-1 (Santa Cruz #sc-107), NF-κB p65 (Cell Signaling #8242S), VE-Cadherin (R&D #AF938). Imaging was performed on a Zeiss LSM 900 confocal microscope equipped with 405nm, 488nm, 561nm and 640 nm laser lines using Plan-Apochromat objectives and Airyscan2 GaAsP-PMT detector. Identical laser intensity settings were applied to samples being compared with equivalent Z thickness. After acquisition, a maximum intensity projection of the Z-stack was applied using ZEN Blue 3.5 software (ZEISS). Image processing and quantification of parameters was performed with ImageJ (NIH).

2.6 Drawings

Schematics in figures were created using BioRender.com.

2.7 Statistical analysis

Statistical analysis was performed using GraphPad Prism software. The results are presented as mean ± SD. The Shapiro-Wilk normality test was conducted to measure normal distribution of dependent variables. For normally distributed data, two-tailed independent *t*-test was used to determine statistically significant differences between two groups. For data that did not pass the normality test, nonparametric one-tailed Mann-Whitney U test was conducted to examine statistical significance between 2 experimental conditions. $p < 0.05$ was considered statistically significant for all analyses.

3 Results

3.1 Disturbed flow alters genes associated with lipid metabolism

HAECs were exposed to UF (20 dyn/cm^2) or DF (±4 dyn/cm^2, 2 Hz) for 48 h and subjected to RNA sequencing (RNAseq) and shotgun lipidomics (Figure 1A). We confirmed the expected difference in cell morphology of HAECs after exposure to UF

10.3389/fphys.2024.1431847

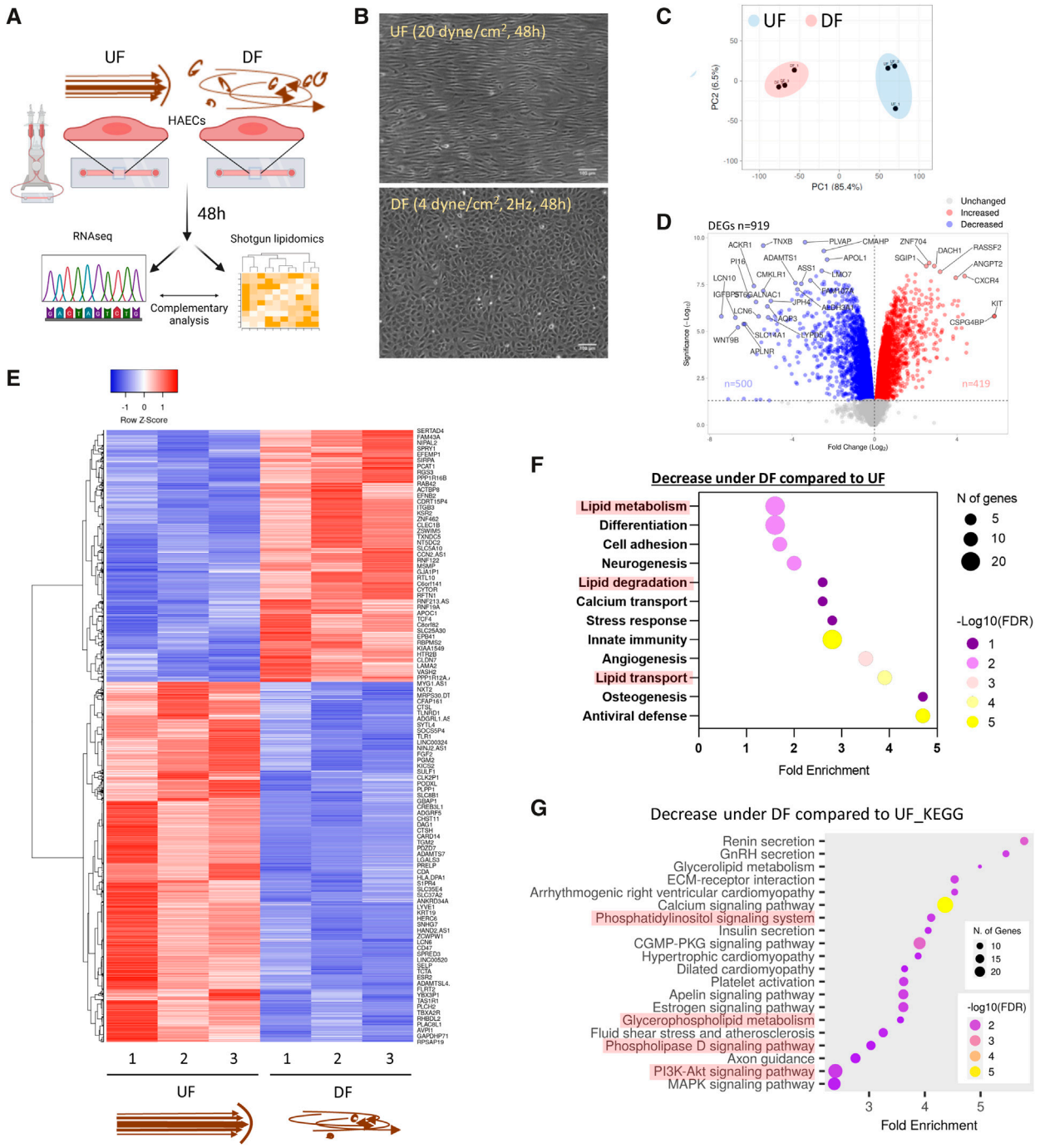

FIGURE 1
Flow pattern affects the transcriptional signature of HAECs and alters the expression of genes related to lipid metabolism **(A)** Schematic diagram of the experimental procedure. **(B)** Brightfield micrographs of HAEC monolayers exposed to UF and DF for 48 h. **(C)** PCA plot of RNA sequencing (RNASeq) data. **(D)** Volcano plot of differentially expressed genes (DEGs). **(E)** Heatmap of DEGs. **(F)** Pathway analysis using DAVID (UniProt database) showing the biological processes downregulated under DF vs. UF. **(G)** Pathway analysis using ShinyGO (KEGG database) to show reduced biological pathways under DF. UF = Unidirectional laminar flow. DF = Disturbed flow.

or DF for 48 h (Figure 1B). To confirm that our *in vitro* flow system generated the expected EC phenotypes under the applied flow conditions, we validated gene and protein expression. The expression levels of known flow-responsive genes, including Kruppel-like Factor 2 (*KLF2*), Kruppel-like Factor 4 (*KLF4*), and Nitric Oxide Synthase 3 (*NOS3*) showed a significant upregulation under UF (Supplementary Figure S1A). In addition, confocal imaging of HAEC monolayers confirmed the increase in eNOS protein expression under UF (Supplementary Figure S1B).

10.3389/fphys.2024.1431847

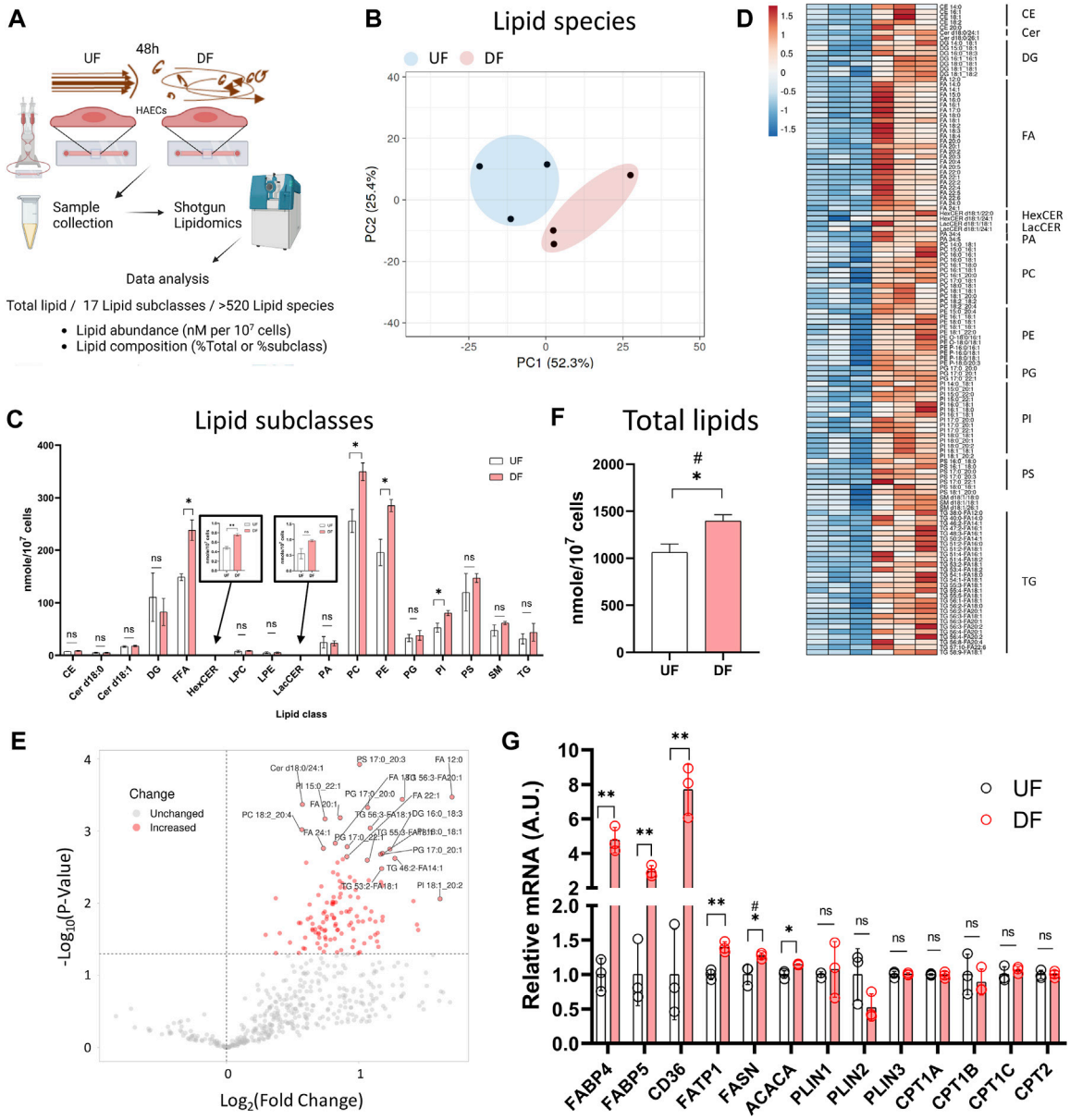

FIGURE 2
Lipid abundance is elevated in HAECs exposed to DF compared to UF **(A)** Schematic diagram of the lipidomics analysis. **(B)** PCA plot of lipidomics data. **(C)** Abundance of each lipid subclasses under UF vs. DF (n = 3). **(D)** Heatmap of altered lipid species for DF vs. UF. **(E)** Volcano plot showing altered lipid species under DF vs. UF. **(F)** Total lipid abundance (nM per 10^7 cells) under UF vs. DF. Total lipid abundance was calculated from lipidomics results (n = 3). **(G)** Expression of the genes involved in fatty acid synthesis, uptake and transport from the RNAseq data (n = 3). Bar graph shown as mean ± SD. *p< 0.05, **p< 0.01, ns = not significant by two-tailed unpaired *t*-test. #p< 0.05 by one-tailed Mann-Whitney U test.

Consistent with previous reports (Tamargo et al., 2023), our RNAseq analysis showed that DF resulted in dramatic changes in the gene expression profile compared to HAECs exposed to UF (Figures 1C–E). Pro-inflammatory genes known to be induced by DF, such as Angiopoietin 2 (*ANGPT2*), Endothelin 1 (*EDN1*), C-C Motif Chemokine Ligand 2 (*CCL2*), NADPH Oxidase 4 (*NOX4*), 6-phosphofructo-2-kinase/fructose-2,6-biphosphatase 3 (*PFKFB3*), and Hypoxia-Inducible-Factor 1A (*HIF1A*) (Doddaballapur et al., 2015; Wu et al., 2017; Maurya et al., 2021), were significantly elevated in HAECs exposed to DF (Supplementary Figure S1C). Additionally, we confirmed the pro-inflammatory phenotype of HAECs exposed to DF by confocal imaging. HAECs exposed to DF had increased nuclear NF-κB p65 localization and ICAM-1 protein expression compared to HAECs exposed to UF (Supplementary Figures S1D, S1E). Pathway analysis of differentially expressed genes for HAECs exposed to DF *versus* UF revealed changes in transcripts associated with lipid metabolism, lipid degradation, lipid transport, and lipid signaling (Figures 1F, G).

3.2 Exposure to disturbed flow increases total cellular lipid content

Based on the observation that genes associated with lipid metabolism were altered in DF compared to UF, we hypothesized that the applied flow pattern may affect the EC lipidome. Therefore, we compared the lipid profiles of HAECs exposed to UF and DF for 48 h (Figure 2A).

Shotgun lipidomics detected a total of 520 individual lipid species from 17 lipid subclasses (Figure 2A). As visualized by principal component analysis (PCA), the lipid profile was distinct between HAECs exposed to UF and DF (Figure 2B). Of the 17 lipid subclasses measured, 5 lipid subclasses were significantly elevated in HAECs exposed to DF compared to UF (Figure 2C). The lipid subclasses that were higher in DF included free fatty acids (FFA), hexosylceramides (HexCER), phosphatidylcholines (PC), phosphatidylethanolamines (PE), and phosphatidylinositols (PI). PC and PE were the most abundant lipid subclasses detected for HAECs under both flow profiles (Figure 2C). A comparison of individual lipid species showed that 66 species were significantly elevated under DF *versus* UF (Figures 2D, E). Furthermore, the total lipid abundance per cell was higher for HAECs exposed to DF compared to UF (Figure 2F).

Further analysis indicated an increase in the abundance of unesterified fatty acids for HAECs exposed to DF (Supplementary Figures S2A, S2B). Fatty acyl chains for phospholipid and glycerolipid synthesis are obtained via import or endogenous synthesis (He et al., 2023) and the fatty acid abundance in cells is affected by proteins that regulate the uptake, synthesis, and transport of fatty acids, as well as proteins that hydrolyze fatty acids from neutral lipids and phospholipids (Supplementary Figure S2D). Cross analysis of the RNAseq data indicated that genes involved in fatty acid synthesis (*ACACA*, *FASN*), fatty acid uptake (*CD36*) and fatty acid transport (*FABP4*, *FABP5*, *FATP1*) were upregulated under DF (Figure 2G). Interestingly, genes involved in lipid catabolic processes, neutral lipid catabolic processes, and fatty acid catabolic processes tended to be reduced in the presence of DF (Supplementary Figures S3A–D). Additionally, GSEA analysis revealed an increase in transcripts related to cholesterol biosynthesis under DF (Supplementary Figure S3E), further suggesting that flow modulates lipid metabolic pathways in HAECs. Together, gene expression analysis indicated a shift towards a program of increased lipid biosynthesis and import, with reduced lipid turnover for HAECs exposed to DF.

Comparing HAECs under static conditions revealed a lipid profile quite distinct from HAECs exposed to either DF or UF (Supplementary Figures S4, S5). PCA of the lipidomics data showed that cells exposed to UF or DF were clearly separated from cells in static conditions on PC1, and cells exposed to DF or static conditions were separated from cells exposed to UF on PC2 (Supplementary Figure S6A). The top 20 lipid species responsible for the separation along PC1 and PC2 are listed in Supplementary Figure S6B. Furthermore, HAECs exposed to DF had more lipid content per cell than HAECs exposed to either UF or static conditions (Supplementary Figure S6C). A heatmap of differentially expressed lipid species showed clear effects of applied flow on the lipid profile of HAECs (Supplementary Figure S6D).

3.3 Specific lipid species are altered by disturbed flow

We next analyzed the lipid composition of cells exposed to DF or UF by expressing each lipid subclass as a percent (%) of total cellular lipids. Despite the increase in total lipid mass per cell in the DF condition, the percent composition of each lipid subclass remained unchanged for HAECs exposed to DF or UF (e.g., PCs accounted for ~25% total cellular lipids in both DF and UF) (Figure 3A). Therefore, we examined whether there was a shift in the contribution of specific lipid species as a fraction of its total subclass. Twenty-three lipid species were increased, and five lipid species were decreased under DF compared to UF (Figures 3B–E). A closer look at the lipid species indicated that phospholipids containing mono-unsaturated fatty acids (MUFA) at the sn-2 position were increased in DF compared to UF (e.g., PE 18:1_18:1, PG 16:0_18:1, PG 18:1_18:1, PI 18:0_18:1, PI 18:0_20:1). Conversely, phospholipid species containing polyunsaturated fatty acids (e.g., PC 18:0_20:4, PE 18:0_20:4, PE 18:0_22:4) were decreased under DF.

3.4 Endothelial lipid profile is altered in response to pro-inflammatory signals

Since DF results in an inflammatory phenotype (Supplementary Figures S1C–E), we asked if specific pro-inflammatory signals also altered the lipid composition of ECs. To address this, we performed shotgun lipidomics on statically cultured HAECs in the absence or presence of the pro-inflammatory agonists Pam3CSK4 (Pam3; Toll-like receptor 1/2 agonist) or lipopolysaccharides (LPS; Toll-like receptor 4 agonist) for 48 h. We first confirmed that exposure to LPS and Pam3 for 48 h at the dosages applied resulted in an inflammatory phenotype by staining for ICAM-1 and NF-κB p65. As expected, HAECs exposed to LPS or Pam3 had increased ICAM-1 and nuclear localization of NF-κB p65 compared to control HAECs (Supplementary Figures S7A–D). As we observed for HAECs exposed to DF, the total lipid abundance per cell was significantly elevated in response to LPS and Pam3 compared to vehicle treated control cells (Figure 4A). Cellular lipidomes were distinct between HAECs treated with pro-inflammatory agonists *versus* control HAECs (Figures 4B, C, E, F). In summary, a total of twelve lipid subclasses were elevated in response to LPS and eight lipid subclasses were elevated in response to Pam3 (Figure 4D). We noted that cholesteryl ester (CE) and sphingomyelin (SM) subclasses were reduced in Pam3-treated HAECs, while CE and SM were increased in response to LPS (Figure 4D). In addition, PCA and hierarchical clustering showed that exposure to inflammatory agonists led to dramatic differences in the cellular lipid composition (Supplementary Figures S7E–I).

3.5 Specific lipid species are elevated in response to disturbed flow and inflammatory agonists

Cross-analysis of the datasets identified lipid species that were altered in the presence of DF and inflammatory agonist

10.3389/fphys.2024.1431847

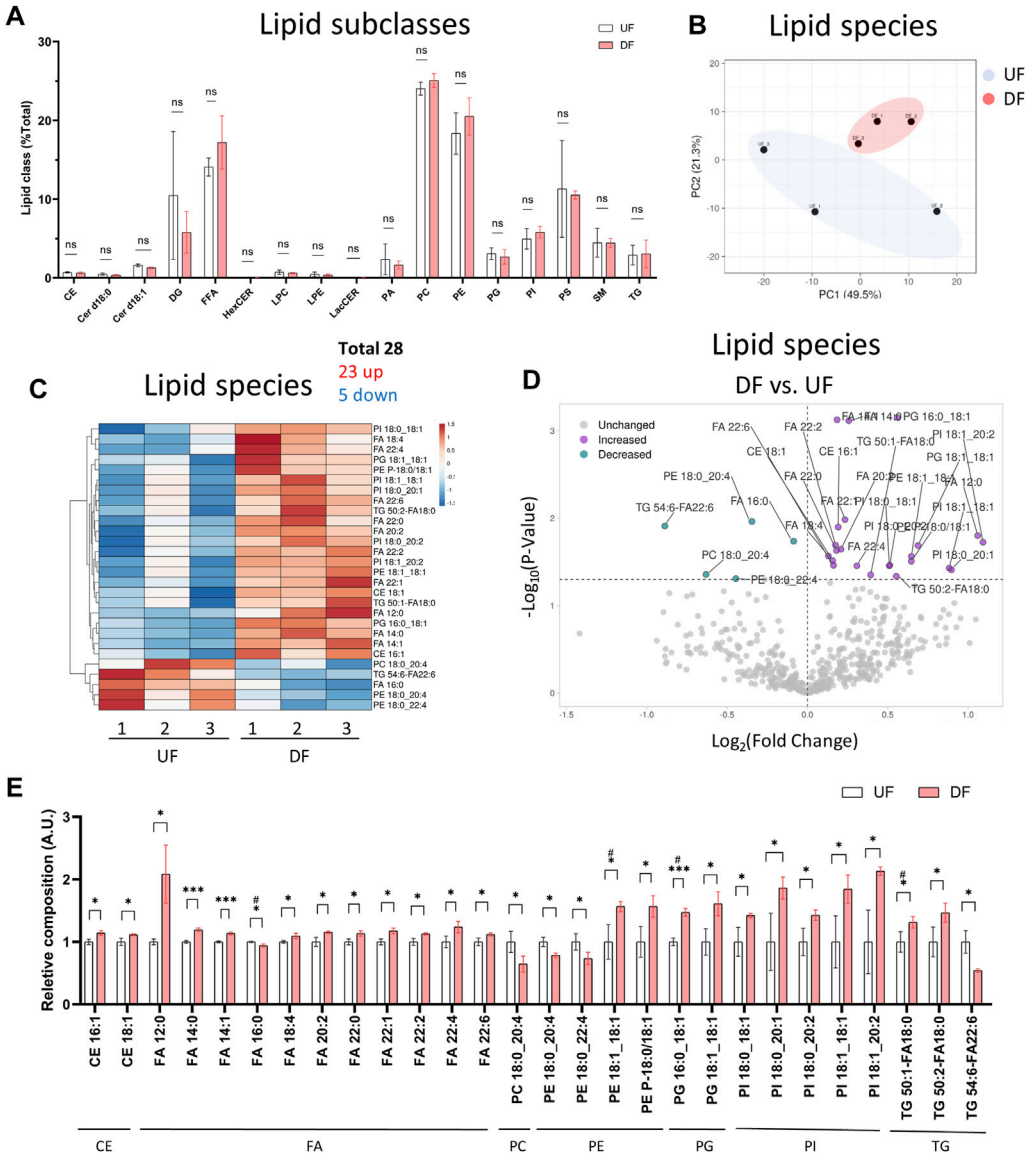

FIGURE 3
Lipid subclass composition is not changed by flow pattern **(A)** Bar graph of lipid subclass composition (lipid subclass/total lipid) for HAECs exposed to UF and DF (n = 3). **(B)** PCA plot using lipid species composition. **(C)** Heatmap of lipid species changed by percent composition under DF vs. UF. **(D)** Volcano plot of lipid species altered in composition. **(E)** Bar graph of lipid species altered in composition under DF vs. UF (n = 3). Bar graph shown as mean ± SD. *p< 0.05, **p< 0.01, ***p< 0.001, ns = not significant by two-tailed unpaired *t*-test. #p< 0.05 by one-tailed Mann-Whitney U test.

exposure. The abundance of 57 lipid species (nMols per cell) were increased in DF, LPS, or Pam3 exposure (Supplementary Figure S8A). However, by percent composition of individual lipid species, quantified as the percent abundance relative to the lipid subclass abundance, only six lipid species were increased in response to DF, LPS and Pam3 (Supplementary Figure S8B). Further analysis revealed that only five lipid species, specifically PE 18:1_18:1, PI 18:0_18:1, PI 18:0_20:2, PI 18:1_18:1, PI 18:1_20:2, were elevated in abundance and percent composition in the presence of DF, LPS, and Pam3 (Figures 5A, C–F). We noted that stearic acid (18:0), oleic acid (18:1), and eicosadienoic acid (20:2), were common to these five lipid species. The total abundance of stearic acid, oleic acid, and eicosadienoic acid was elevated in response to DF and inflammatory agonists (Figure 5B). We further noted that four out of the five lipids that increased in absolute mass and percent of total lipid class by DF, LPS, and Pam3 were PI species. This observation was consistent with pathway enrichment scores for PI signaling and metabolism from the RNASeq data for HAECs exposed to DF (Supplementary Figure S9).

3.6 Monounsaturated fatty acid incorporation into phospholipids at the sn-2 position is enhanced with disturbed flow

We subsequently investigated the acyl tail compositions of fatty acids incorporated at the sn-2 position in phospholipids for cells

10.3389/fphys.2024.1431847

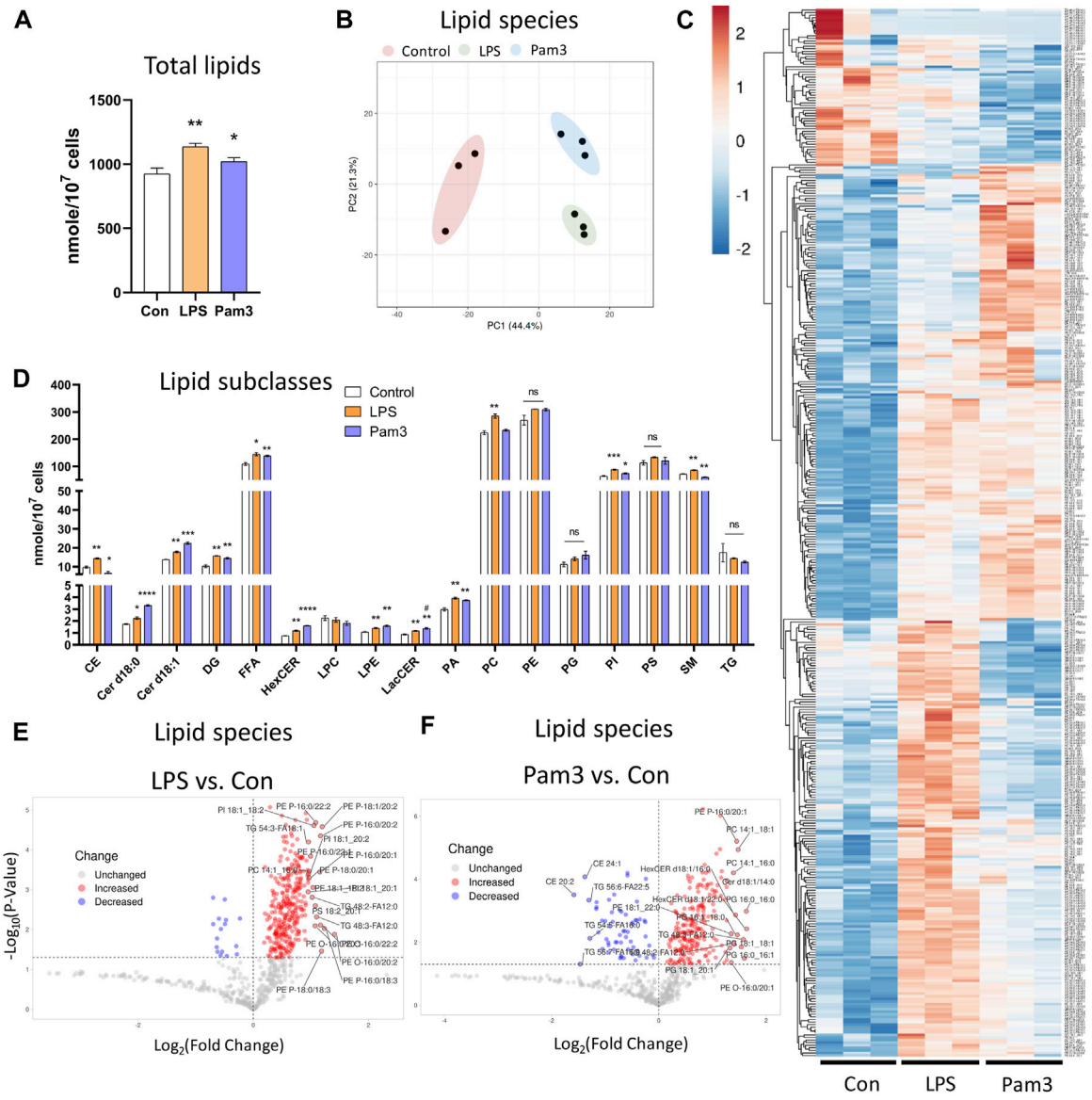

FIGURE 4
Lipid profile is altered in response to inflammatory agonist exposure **(A)** Total lipid abundance (nM per 10^7 cells) in HAECs treated with vehicle (control), LPS, and Pam3. Total lipid abundance was calculated from lipidomics results (n = 3). **(B)** PCA plot. Red = control HAECs, Green = LPS-treated HAECs, Blue = Pam3-treated HAECs. **(C)** Heatmap of altered lipid species in composition in response to vehicle, LPS, and Pam3. **(D)** Bar plot of lipid subclass abundance in control, LPS, and Pam3 groups (n = 3). **(E)** Volcano plot of lipid species changed in LPS vs. control. **(F)** Volcano plot of lipid species changed in Pam3 vs. control. Bar graph shown as mean ± SD. *p< 0.05, **p< 0.01, ***p< 0.001, ns = not significant by two-tailed unpaired *t*-test. #p< 0.05 by one-tailed Mann-Whitney U test.

exposed to DF and UF. Comparing the altered phospholipid species by abundance, we found that ~61% of the phospholipids contained MUFAs at the sn-2 position, while ~24% contained a saturated fatty acid (SFA) and ~14% contained a polyunsaturated fatty acid (PUFA) (Figures 6A, B). Over half of the phospholipids that were significantly changed in DF by composition contained a MUFA and 42% contained a PUFA at the sn-2 position (Figures 6B, C).

Phospholipids are produced by *de novo* synthesis and their fatty acyl chains can subsequently be remodeled by Land's cycle, which involves removing a fatty acid from the sn-2 position by phospholipase A2 before re-acylating it by lysophospholipid acyltransferases (LPLATs) (Shindou et al., 2013) (Figure 6D). Therefore, the observed changes in phospholipid composition of membranes under DF compared to UF could be due to (1) altered uptake or synthesis of fatty acids for *de novo* phospholipid production or (2) changes in phospholipid remodeling.

From the RNASeq data, we observed higher expression of the fatty acid transporter *CD36*, a major route of fatty acid uptake, for HAECs under DF (Figure 2H). Additionally, the sequencing data indicated that genes involved in SFA and MUFA synthesis, including *FASN*, *ACACA*, and Stearoyl-CoA Desaturase 5 (*SCD5*) were significantly increased for HAECs exposed to DF

10.3389/fphys.2024.1431847

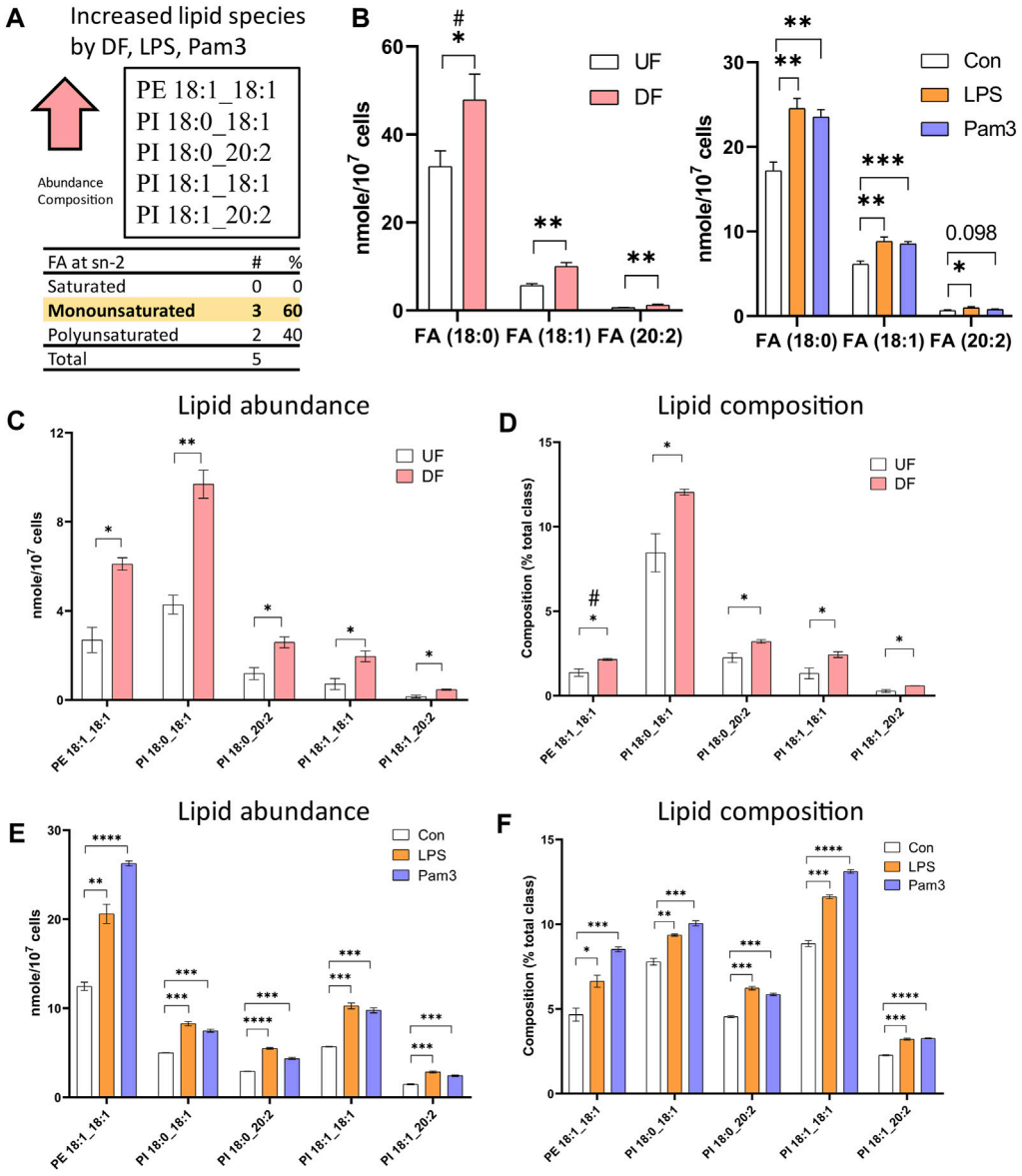

FIGURE 5
Specific lipid species are increased in HAECs exposed to disturbed flow or inflammatory agonists **(A)** Summary of cross analysis from the lipidomics datasets. Five lipid species (PE 18:1_18:1, PI 18:0_18:1, PI 18:0_20:2, PI 18:1_18:1, PI 18:1_20:2) were significantly elevated in abundance and percent composition for HAECs exposed to either DF or inflammatory agonist treatment. **(B)** Abundance of fatty acids incorporated into the lipid species identified in **(A)** for HAECs under UF and DF or HAECs exposed to vehicle (control), LPS, and Pam3 treatments (n = 3). **(C)** Lipid abundance of the shared lipid species in HAECs under UF vs. DF (n = 3). **(D)** Lipid composition of the shared lipid species in HAECs under UF vs. DF (n = 3). **(E)** Lipid abundance of the shared lipid species in HAECs in response to vehicle, LPS, and Pam3 (n = 3). **(F)** Lipid composition of the commonly shared lipid species for HAECs in response to vehicle, LPS, and Pam3 (n = 3). Bar graph shown as mean ± SD. *p< 0.05, **p< 0.01, ***p< 0.001, ****p< 0.001, ns = not significant by two-tailed unpaired *t*-test. #p< 0.05 by one-tailed Mann-Whitney U test.

(Figure 6G). The RNASeq data suggests that higher *de novo* MUFA synthesis could contribute to the increased abundance of MUFA-containing phospholipids under DF. The data also showed that the expression levels of select LPLATs were changed under DF compared to UF (Figure 6E). Specifically, gene expression of the membrane bound O-acyltransferase domain-containing 7 (*MBOAT7*)/lysophosphatidylinositol acyltransferase 1 (*LPIAT1*), an enzyme involved in PI remodeling (Shindou et al., 2009; Shindou et al., 2013; Tanaka et al., 2021), and lysophosphatidylcholine acyltransferase 2 (*LPCAT2*), which remodels platelet-activating factor (PAF) and PC (Shindou et al., 2009; Shindou et al., 2013), were significantly upregulated under DF. Together, the observations suggest that changes in fatty acid import and synthesis, combined with changes in the phospholipid remodeling machinery (Figure 6F), could contribute to the changes in phospholipid species composition for HAECs exposed to DF compared to UF.

The top 20 phospholipid species used for the PCA loadings for PC1 are listed in Supplementary Figures S10A, S10B. Notably,

10.3389/fphys.2024.1431847

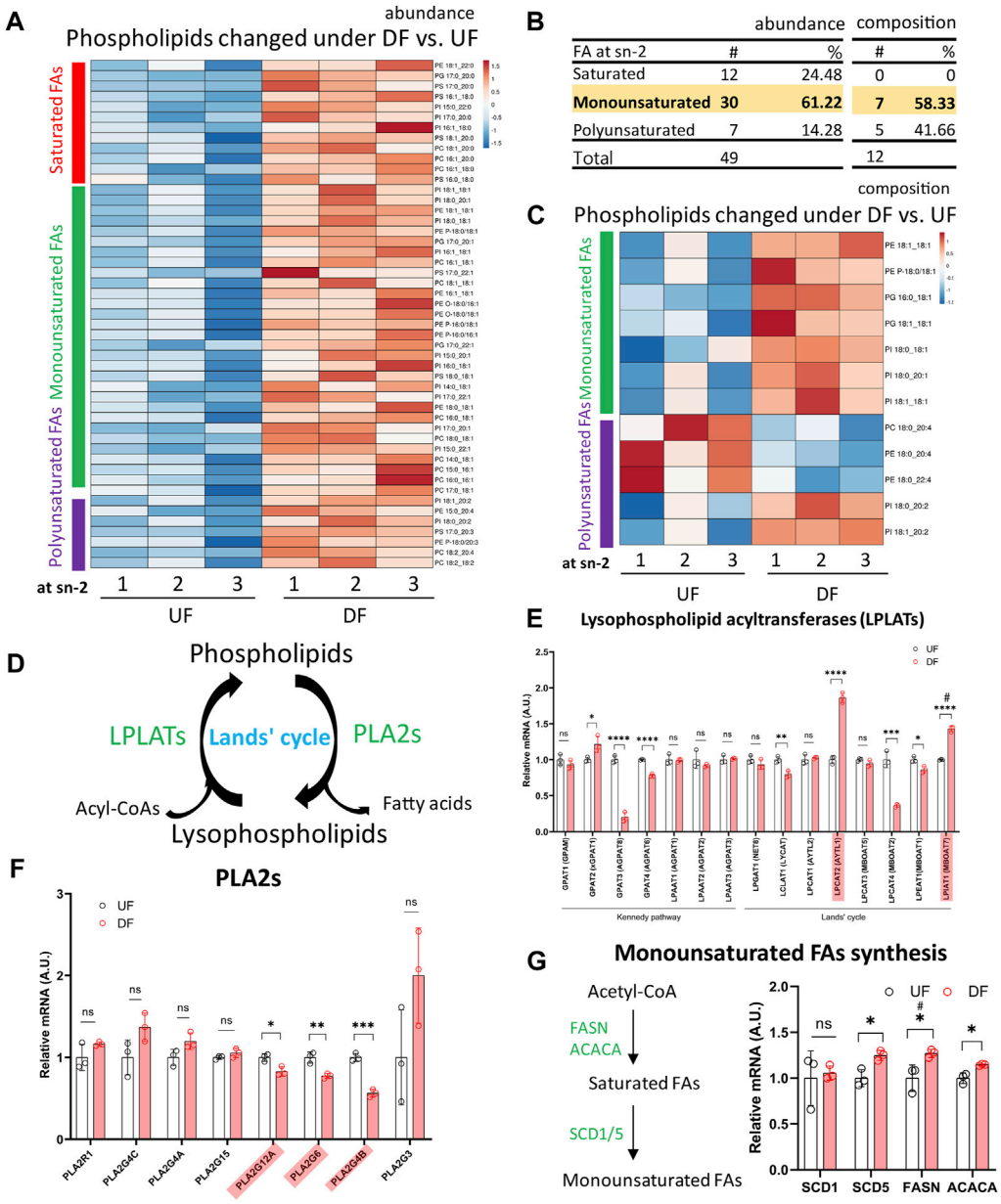

FIGURE 6
Incorporation of monounsaturated fatty acids into phospholipids at the sn-2 position was enhanced under DF **(A)** Heatmap of phospholipids altered in abundance under DF vs. UF. **(B)** Table listing the fatty acid incorporated at the sn-2 position of altered phospholipids. Values of abundance from **(A)** and values of composition from **(C)**. **(C)** Heatmap of phospholipids changed in composition under DF vs. UF. **(A, C)** Color bars represent fatty acid type located at the sn-2 position. Red = saturated, Green = monounsaturated, Purple = polyunsaturated. **(D)** Schematic diagram of Lands' cycle. Data from RNAseq dataset for HAECs under DF vs. UF showing **(E)** gene expression of Lysophospholipid acyltransferases (LPLATs), **(F)** gene expression of Phospholipase A2 (PLA2s) isoforms and **(G)** genes associated with monounsaturated fatty acid synthesis (n = 3). Bar graph shown as mean ± SD. *p< 0.05, **p< 0.01, ***p< 0.001, ****p< 0.001, ns = not significant by two-tailed unpaired *t*-test. #p< 0.05 by one-tailed Mann-Whitney U test.

MUFAs were the dominant acyl tails incorporated at the sn-2 position of the top 20 phospholipid species under both DF (65%) and LPS/Pam3 stimulation (45%), as assessed by PCA analysis. Additionally, the abundance of MUFAs in phospholipids was significantly increased after exposure to DF and pro-inflammatory agonists (Supplementary Figures S10C–H), suggesting a shift towards a program of increased MUFA synthesis and/or FA import.

4 Discussion

In this study, we found that the applied flow pattern (DF *versus* UF) distinctively alters the EC transcriptome and lipidome. While previous reports have shown that laminar shear stress alters the lipidome of pulmonary artery ECs (Hirata et al., 2021), this is the first report to correlate how flow pattern affects metabolic gene expression and lipidomic profiles of arterial ECs. Using RNA

sequencing and shotgun lipidomics, we found that HAECs exposed to DF have an inflammatory transcriptional signature and increased cellular lipid content compared to HAECs exposed to UF. By exposing HAECs to inflammatory agonists, Pam3 or LPS, we confirmed that the EC inflammatory state is associated with higher lipid accumulation. Increased lipid accumulation has previously been reported in other cell types exposed to stress conditions, including viral infection-mediated inflammation (Prado et al., 2023). Furthermore, in human microvascular ECs, the expression of the FA transporter CD36 increased in response to viral infection (Sato and Coburn, 2017). Analysis of our RNA sequencing data for DF *versus* UF revealed that genes involved in fatty acid synthesis (*FASN* and *ACACA*), and fatty acid transport (*CD36* and *FATP1*), were upregulated, while genes involved in lipid and fatty acid catabolic processes were reduced. These transcriptional changes suggest that DF may induce changes in the rate of lipid uptake and synthesis to supply more fatty acids for phospholipid and neutral lipid synthesis.

Considering the increased lipid load, it is interesting to consider whether altering lipogenesis in the presence of an inflammatory stimulus would alter the EC phenotype. Previous studies have shown that increasing *de novo* MUFA synthesis by Stearoyl-CoA Desaturases (SCDs) can modulate vascular inflammation, where an attenuation of MUFA synthesis by inhibition of endothelial SCD1 activity stimulated the secretion of pro-inflammatory cytokines and elevated inflammation in the mouse aorta (MacDonald et al., 2009; Cavallero et al., 2024). Therefore, it is conceivable that inhibition of *de novo* lipogenesis, a step upstream of SCDs, by pharmacological inhibition or by deletion of Fatty Acid Synthase could also alter the EC phenotype in response to DF. However, we note the critical role of *de novo* lipogenesis in the context of angiogenesis, eNOS activity, and permeability (Wei et al., 2011; Bruning et al., 2018), therefore, inhibition of lipogenesis could have broad consequences. It is also likely that a major contributor to the increase in EC fatty acid content in an inflammatory setting is the increase in CD36, which transports fatty acids into cells. Inhibition of lipogenesis alone may not be sufficient to block the increase in cellular fatty acids after exposure to DF. Future studies are needed to dissect the impact of the observed elevation of lipids in response to inflammatory stimuli in ECs. Additionally, experiments using stable isotope tracing to measure the contribution of long chain SFA and MUFA synthesis for the observed altered phospholipid composition in response to DF will enable quantification of EC lipid uptake and synthesis.

Exposure of HAECs to DF or an inflammatory agonist, either LPS or Pam3, led to an increase in the abundance of MUFA-containing phospholipids. We noted that genes involved in SFA and MUFA synthesis, including *FASN*, *ACACA* and *SCD5,* were elevated under DF. Stearoyl Coenzyme A (CoA) desaturases incorporates a Δ9-cis-double bond into SFA-CoA to make MUFAs (Igal and Sinner, 2021), and MUFAs have been reported to counteract membrane stress induced by SFAs (Hardy et al., 2000; Koeberle et al., 2016). Furthermore, MUFAs have been shown to play a role in the modulation of various stress signaling pathways (Koeberle et al., 2015; Koeberle et al., 2016; Magtanong et al., 2019; Tesfay et al., 2019; Igal and Sinner, 2021). In fact, a recent study in macrophages found that Toll-like receptor-agonist exposure increased *de novo* MUFA synthesis and that attenuating MUFA synthesis with inhibition of SCDs led to heightened inflammation (Hsieh et al., 2020). Therefore, the observed increase in MUFA-containing phospholipid content in response to DF in ECs could be a compensatory mechanism to alleviate the DF-induced inflammatory state. Examination of the mechanisms by which MUFA-containing phospholipid content is increased in response to inflammatory agonists or DF, and the specific pathways that are modulated by MUFA-containing phospholipids, is warranted.

The lipidomics data revealed an increase in the major membrane lipids PC and PE for HAECs exposed to DF compared to UF. Notably, the total unesterified fatty acid content of cells exposed to DF was higher. This increase in PC and PE content could be driven by increased fatty acid import via *CD36* or higher *de novo* fatty acid synthesis, since fatty acid availability drives phospholipid synthesis (Pelech et al., 1983). Another possible explanation for the increased pool size of PC and PE is the expansion of cellular organelle volume and/or organelle number in ECs under DF. In fact, athero-susceptible shear stress has been reported to induce ER stress and ER expansion, thereby leading to EC dysfunction and inflammation (Bailey et al., 2017). However, future studies are required to investigate these possible scenarios and the functional importance of increased PC and PE content in ECs exposed to DF.

Finally, we identified five lipid species (PE 18:1_18:1, PI 18:0_18:1, PI 18:0_20:2, PI 18:1_18:1, PI 18:1_20:2) that were significantly elevated in abundance and percent composition for HAECs exposed to DF and inflammatory agonist treatment. We noted that the total abundance of the fatty acids incorporated into those lipid species– stearic acid, oleic acid and eicosadienoic acid– were elevated in cells exposed to DF and exposure to inflammatory agonists. By RNA sequencing, we observed altered expression of genes related to PI signaling and metabolism under DF. While the role of PI metabolism on cellular stress signaling has not been examined in detail in ECs, a recent study showed that the SCD1-derived 'lipokine' PI 18:1_18:1 suppressed stress signaling in fibroblasts (Thurmer et al., 2022). The results in fibroblasts indicated that PI 18:1_18:1 was elevated in response to cytotoxic stressors and prevented p38 MAPK activation and impeded the unfolded protein response (Thurmer et al., 2022). Future studies are needed to determine how our observed changes in the abundance of PI species in response to DF affects signaling in ECs.

We note that our *in vitro* flow system using parallel plate flow chambers does not recapitulate the physiological oscillatory disturbed flow patterns of the aortic arch. However, considering the limitations of *in vitro* models, we confirmed that using the ibidi μ-slide flow chambers under continuous uni-directional laminar flow (20 dyn/cm^2) and oscillatory flow (4 dyn/cm^2, 2 Hz) effectively provided athero-protective and athero-prone phenotypes as evidenced by EC cell morphology, gene expression, and protein expression. We also note that HAECs from one single healthy donor were used throughout this study. The choice of a single donor was to provide technical replicates for the changes in gene expression and lipids across treatments. Future work is certainly warranted to investigate how variations in genetics affect the gene expression and lipid responses across multiple donor HAECs in the context of aging and genetic backgrounds.

5 Conclusion

In conclusion, we provide transcriptomic and lipidomic datasets of HAECs under athero-protective UF and athero-prone DF patterns. Additionally, we map the lipidome of HAECs after exposure to the inflammatory agonists LPS and Pam3. We anticipate that these datasets will be a useful resource for the vascular biology community to be further dissected and advance our understanding of how flow pattern influences the EC phenotype.

Data availability statement

The RNA sequencing data has been deposited in NCBI's Gene Expression Omnibus repository (GSE266437). Normalized RNA sequencing data and the lipidomics data are provided as an Excel file in the Supplementary Material.

Ethics statement

Ethical approval was not required for the studies on humans in accordance with the local legislation and institutional requirements because only commercially available cell lines were used.

Author contributions

S-GH: Conceptualization, Data curation, Formal Analysis, Investigation, Methodology, Project administration, Validation, Visualization, Writing–original draft, Writing–review and editing. JK: Visualization, Writing–review and editing. KW: Data curation, Formal Analysis, Investigation, Methodology, Writing–review and editing. SB: Methodology, Resources, Supervision, Writing–review and editing. JM: Conceptualization, Funding acquisition, Investigation, Project administration, Supervision, Writing–original draft, Writing–review and editing.

Funding

The author(s) declare that financial support was received for the research, authorship, and/or publication of this article. This work was funded by the National Center for Advancing Translational Sciences UCLA CTSI Grant UL1TR001881 and NIH grant P30 DK063491. S-GH was supported as a Jim Easton CDF Investigator; JK was supported by AHA Postdoctoral Fellowship 903306; SB was supported by NIH grant R01HL157710; JM was supported by American Heart Association Career Development Award 19CDA34760007.

Acknowledgments

The content of this manuscript has previously appeared online as a preprint on bioRxiv, the preprint server for biology (Hong et al., 2024).

Conflict of interest

The authors declare that the research was conducted in the absence of any commercial or financial relationships that could be construed as a potential conflict of interest.

Publisher's note

Supplementary material

The Supplementary Material for this article can be found online at: https://www.frontiersin.org/articles/10.3389/fphys.2024.1431847/full#supplementary-material

References

Babicki, S., Arndt, D., Marcu, A., Liang, Y., Grant, J. R., Maciejewski, A., et al. (2016). Heatmapper: web-enabled heat mapping for all. *Nucleic Acids Res.* 44, W147–W153. doi:10.1093/nar/gkw419

Bailey, K. A., Haj, F. G., Simon, S. I., and Passerini, A. G. (2017). Atherosusceptible shear stress activates endoplasmic reticulum stress to promote endothelial inflammation. *Sci. Rep.* 7, 8196. doi:10.1038/s41598-017-08417-9

Bruning, U., Morales-Rodriguez, F., Kalucka, J., Goveia, J., Taverna, F., Queiroz, K. C. S., et al. (2018). Impairment of angiogenesis by fatty acid synthase inhibition involves mTOR malonylation. *Cell. Metab.* 28, 866–880. doi:10.1016/j.cmet.2018.07.019

Cavallero, S., Roustaei, M., Satta, S., Cho, J. M., Phan, H., Baek, K. I., et al. (2024). Exercise mitigates flow recirculation and activates metabolic transducer SCD1 to catalyze vascular protective metabolites. *Sci. Adv.* 10, eadj7481. doi:10.1126/sciadv.adj7481

Chiu, J. J., and Chien, S. (2011). Effects of disturbed flow on vascular endothelium: pathophysiological basis and clinical perspectives. *Physiol. Rev.* 91, 327–387. doi:10.1152/physrev.00047.2009

Davis, M. E., Cai, H., Drummond, G. R., and Harrison, D. G. (2001). Shear stress regulates endothelial nitric oxide synthase expression through c-Src by divergent signaling pathways. *Circ. Res.* 89, 1073–1080. doi:10.1161/hh2301.100806

Dobin, A., Davis, C. A., Schlesinger, F., Drenkow, J., Zaleski, C., Jha, S., et al. (2013). STAR: ultrafast universal RNA-seq aligner. *Bioinformatics* 29, 15–21. doi:10.1093/bioinformatics/bts635

Doddaballapur, A., Michalik, K. M., Manavski, Y., Lucas, T., Houtkooper, R. H., You, X., et al. (2015). Laminar shear stress inhibits endothelial cell metabolism via KLF2-mediated repression of PFKFB3. *Arterioscler. Thromb. Vasc. Biol.* 35, 137–145. doi:10.1161/ATVBAHA.114.304277

Galley, H. F., and Webster, N. R. (2004). Physiology of the endothelium. *Br. J. Anaesth.* 93, 105–113. doi:10.1093/bja/aeh163

Ge, S. X., Jung, D., and Yao, R. (2020). ShinyGO: a graphical gene-set enrichment tool for animals and plants. *Bioinformatics* 36, 2628–2629. doi:10.1093/bioinformatics/btz931

Goodman, J. M. (2008). The gregarious lipid droplet. *J. Biol. Chem.* 283, 28005–28009. doi:10.1074/jbc.R800042200

Hardy, S., Langelier, Y., and Prentki, M. (2000). Oleate activates phosphatidylinositol 3-kinase and promotes proliferation and reduces apoptosis of MDA-MB-231 breast cancer cells, whereas palmitate has opposite effects. *Cancer Res.* 60, 6353–6358.

Heberle, H., Meirelles, G. V., Da Silva, F. R., Telles, G. P., and Minghim, R. (2015). InteractiVenn: a web-based tool for the analysis of sets through Venn diagrams. *BMC Bioinforma.* 16, 169. doi:10.1186/s12859-015-0611-3

He, Q., Chen, Y., Wang, Z., He, H., and Yu, P. (2023). Cellular uptake, metabolism and sensing of long-chain fatty acids. *Front. Biosci.* 28, 10. doi:10.31083/j.fbl2801010

Hirata, T., Yamamoto, K., Ikeda, K., and Arita, M. (2021). Functional lipidomics of vascular endothelial cells in response to laminar shear stress. *FASEB J.* 35, e21301. doi:10.1096/fj.202002144R

Hong, S.-G., Kennelly, J. P., Williams, K. J., Bensinger, S. J., and Mack, J. J. (2024). Flow-mediated modulation of the endothelial cell lipidome. *bioRxiv* 2024.

Hsieh, W. Y., Williams, K. J., Su, B., and Bensinger, S. J. (2021). Profiling of mouse macrophage lipidome using direct infusion shotgun mass spectrometry. *Star. Protoc.* 2, 100235. doi:10.1016/j.xpro.2020.100235

Hsieh, W. Y., Zhou, Q. D., York, A. G., Williams, K. J., Scumpia, P. O., Kronenberger, E. B., et al. (2020). Toll-like receptors induce signal-specific reprogramming of the macrophage lipidome. *Cell. Metab.* 32, 128–143. doi:10.1016/j.cmet.2020.05.003

Igal, R. A., and Sinner, D. I. (2021). Stearoyl-CoA desaturase 5 (SCD5), a Delta-9 fatty acyl desaturase in search of a function. *Biochim. Biophys. Acta Mol. Cell. Biol. Lipids* 1866, 158840. doi:10.1016/j.bbalip.2020.158840

Immanuel, J., and Yun, S. (2023). Vascular inflammatory diseases and endothelial phenotypes. *Cells* 12, 1640. doi:10.3390/cells12121640

Koeberle, A., Loser, K., and Thurmer, M. (2016). Stearoyl-CoA desaturase-1 and adaptive stress signaling. *Biochim. Biophys. Acta* 1861, 1719–1726. doi:10.1016/j.bbalip.2016.08.009

Koeberle, A., Pergola, C., Shindou, H., Koeberle, S. C., Shimizu, T., Laufer, S. A., et al. (2015). Role of p38 mitogen-activated protein kinase in linking stearoyl-CoA desaturase-1 activity with endoplasmic reticulum homeostasis. *FASEB J.* 29, 2439–2449. doi:10.1096/fj.14-268474

Macdonald, M. L., Van Eck, M., Hildebrand, R. B., Wong, B. W., Bissada, N., Ruddle, P., et al. (2009). Despite antiatherogenic metabolic characteristics, SCD1-deficient mice have increased inflammation and atherosclerosis. *Arterioscler. Thromb. Vasc. Biol.* 29, 341–347. doi:10.1161/ATVBAHA.108.181099

Magtanong, L., Ko, P. J., To, M., Cao, J. Y., Forcina, G. C., Tarangelo, A., et al. (2019). Exogenous monounsaturated fatty acids promote a ferroptosis-resistant cell state. *Cell. Chem. Biol.* 26, 420–432. doi:10.1016/j.chembiol.2018.11.016

Malek, A. M., Alper, S. L., and Izumo, S. (1999). Hemodynamic shear stress and its role in atherosclerosis. *JAMA* 282, 2035–2042. doi:10.1001/jama.282.21.2035

Maurya, M. R., Gupta, S., Li, J. Y., Ajami, N. E., Chen, Z. B., Shyy, J. Y., et al. (2021). Longitudinal shear stress response in human endothelial cells to atheroprone and atheroprotective conditions. *Proc. Natl. Acad. Sci. U S A* 118, e2023236118. doi:10.1073/pnas.2023236118

Metsalu, T., and Vilo, J. (2015). ClustVis: a web tool for visualizing clustering of multivariate data using Principal Component Analysis and heatmap. *Nucleic Acids Res.* 43, W566–W570. doi:10.1093/nar/gkv468

Muro, E., Atilla-Gokcumen, G. E., and Eggert, U. S. (2014). Lipids in cell biology: how can we understand them better? *Mol. Biol. Cell.* 25, 1819–1823. doi:10.1091/mbc.E13-09-0516

Mutlu, A. S., Duffy, J., and Wang, M. C. (2021). Lipid metabolism and lipid signals in aging and longevity. *Dev. Cell.* 56, 1394–1407. doi:10.1016/j.devcel.2021.03.034

Pelech, S. L., Pritchard, P. H., Brindley, D. N., and Vance, D. E. (1983). Fatty acids promote translocation of CTP:phosphocholine cytidylyltransferase to the endoplasmic reticulum and stimulate rat hepatic phosphatidylcholine synthesis. *J. Biol. Chem.* 258, 6782–6788. doi:10.1016/s0021-9258(18)32290-7

Prado, L. G., Camara, N. O. S., and Barbosa, A. S. (2023). Cell lipid biology in infections: an overview. *Front. Cell. Infect. Microbiol.* 13, 1148383. doi:10.3389/fcimb.2023.1148383

Sakuragi, T., and Nagata, S. (2023). Regulation of phospholipid distribution in the lipid bilayer by flippases and scramblases. *Nat. Rev. Mol. Cell. Biol.* 24, 576–596. doi:10.1038/s41580-023-00604-z

Sato, H., and Coburn, J. (2017). Leptospira interrogans causes quantitative and morphological disturbances in adherens junctions and other biological groups of proteins in human endothelial cells. *PLoS Negl. Trop. Dis.* 11, e0005830. doi:10.1371/journal.pntd.0005830

Shindou, H., Hishikawa, D., Harayama, T., Eto, M., and Shimizu, T. (2013). Generation of membrane diversity by lysophospholipid acyltransferases. *J. Biochem.* 154, 21–28. doi:10.1093/jb/mvt048

Shindou, H., Hishikawa, D., Harayama, T., Yuki, K., and Shimizu, T. (2009). Recent progress on acyl CoA: lysophospholipid acyltransferase research. *J. Lipid Res.* 50, S46–S51. doi:10.1194/jlr.R800035-JLR200

Su, B., Bettcher, L. F., Hsieh, W. Y., Hornburg, D., Pearson, M. J., Blomberg, N., et al. (2021). A DMS shotgun lipidomics workflow application to facilitate high-throughput, comprehensive lipidomics. *J. Am. Soc. Mass Spectrom.* 32, 2655–2663. doi:10.1021/jasms.1c00203

Tamargo, I. A., Baek, K. I., Kim, Y., Park, C., and Jo, H. (2023). Flow-induced reprogramming of endothelial cells in atherosclerosis. *Nat. Rev. Cardiol.* 20, 738–753. doi:10.1038/s41569-023-00883-1

Tanaka, Y., Shimanaka, Y., Caddeo, A., Kubo, T., Mao, Y., Kubota, T., et al. (2021). LPIAT1/MBOAT7 depletion increases triglyceride synthesis fueled by high phosphatidylinositol turnover. *Gut* 70, 180–193. doi:10.1136/gutjnl-2020-320646

Tesfay, L., Paul, B. T., Konstorum, A., Deng, Z., Cox, A. O., Lee, J., et al. (2019). Stearoyl-CoA desaturase 1 protects ovarian cancer cells from ferroptotic cell death. *Cancer Res.* 79, 5355–5366. doi:10.1158/0008-5472.CAN-19-0369

Thurmer, M., Gollowitzer, A., Pein, H., Neukirch, K., Gelmez, E., Waltl, L., et al. (2022). PI(18:1/18:1) is a SCD1-derived lipokine that limits stress signaling. *Nat. Commun.* 13, 2982. doi:10.1038/s41467-022-30374-9

Wei, X., Schneider, J. G., Shenouda, S. M., Lee, A., Towler, D. A., Chakravarthy, M. V., et al. (2011). *De novo* lipogenesis maintains vascular homeostasis through endothelial nitric-oxide synthase (eNOS) palmitoylation. *J. Biol. Chem.* 286, 2933–2945. doi:10.1074/jbc.M110.193037

Wu, D., Huang, R. T., Hamanaka, R. B., Krause, M., Oh, M. J., Kuo, C. H., et al. (2017). HIF-1α is required for disturbed flow-induced metabolic reprogramming in human and porcine vascular endothelium. *Elife* 6, e25217. doi:10.7554/eLife.25217

Yamamoto, K., and Ando, J. (2013). Endothelial cell and model membranes respond to shear stress by rapidly decreasing the order of their lipid phases. *J. Cell. Sci.* 126, 1227–1234. doi:10.1242/jcs.119628

Yamamoto, K., Nogimori, Y., Imamura, H., and Ando, J. (2020). Shear stress activates mitochondrial oxidative phosphorylation by reducing plasma membrane cholesterol in vascular endothelial cells. *Proc. Natl. Acad. Sci. U S A* 117, 33660–33667. doi:10.1073/pnas.2014029117

Yurdagul, A., JR., Finney, A. C., Woolard, M. D., and Orr, A. W. (2016). The arterial microenvironment: the where and why of atherosclerosis. *Biochem. J.* 473, 1281–1295. doi:10.1042/BJ20150844